

RESEARCH

Open Access

Instantaneous frequency based newborn EEG seizure characterisation

Mostefa Mesbah^{1,2*}, John M O' Toole^{1,3}, Paul B Colditz¹ and Boualem Boashash^{1,4}

Abstract

The electroencephalogram (EEG), used to noninvasively monitor brain activity, remains the most reliable tool in the diagnosis of neonatal seizures. Due to their nonstationary and multi-component nature, newborn EEG seizures are better represented in the joint time–frequency domain than in either the time domain or the frequency domain. Characterising newborn EEG seizure nonstationarities helps to better understand their time-varying nature and, therefore, allow developing efficient signal processing methods for both modelling and seizure detection and classification. In this article, we used the instantaneous frequency (IF) extracted from a time–frequency distribution to characterise newborn EEG seizures. We fitted four frequency modulated (FM) models to the extracted IFs, namely a linear FM, a piecewise-linear FM, a sinusoidal FM, and a hyperbolic FM. Using a database of 30-s EEG seizure epochs acquired from 35 newborns, we were able to show that, depending on EEG channel, the sinusoidal and piecewise-linear FM models best fitted 80–98% of seizure epochs. To further characterise the EEG seizures, we calculated the mean frequency and frequency span of the extracted IFs. We showed that in the majority of the cases (>95%), the mean frequency resides in the 0.6–3 Hz band with a frequency span of 0.2–1 Hz. In terms of the frequency of occurrence of the four seizure models, the statistical analysis showed that there is no significant difference ($p = 0.332$) between the two hemispheres. The results also indicate that there is no significant differences between the two hemispheres in terms of the mean frequency ($p = 0.186$) and the frequency span ($p = 0.302$).

Introduction

Seizures tend to happen more frequently in the neonatal period than at any other stage in life [1]. The reported incidence of seizure ranges from 1 to 3 per 1 000 live births in term infants and 10 to 15 per 1 000 live births in preterm infants [2]. Seizures usually arise as the result of excessive, synchronous electrical discharge, of neurons within the central nervous system [3,4]. Although not a disease in themselves, seizures are the most prominent manifestation of neurological dysfunction in the newborn [4]. They often suggest underlying disease processes which may cause irreversible damage to the developing neonatal brains and have demonstrated association with infant mortality and long term morbidity [5]. The underlying brain conditions associated with seizures in the neonates include hypoxic-ischemic encephalopathy, brain

haemorrhage, stroke and meningitis [6,7]. It is therefore critical to recognise neonatal seizures in their early stages to allow timely medical intervention. Clinical assessment of seizures in the neonates is difficult and unreliable as many neonatal seizures occur either in the absence of any clinical signs or accompanied by only subtle ones [8,9]. The clinical diagnosis is further hampered by the frequent administration of sedative or paralytic agents to the newborn patients in neonatal intensive care units.

Recorded via electrodes attached to the scalp, electroencephalogram (EEG) noninvasively measures the electrical activities of the brain and provides useful information about its state. In the neonates, EEG is often the first test to reveal clinically unsuspected seizures and remains the only reliable method for the identification and diagnosis of subclinical seizures [10]. Besides being an effective tool for diagnosis, newborn EEG also correlates with long-term neurodevelopment outcome [11]. EEG analysis can also assist in the design of automated methods for seizure detection, classification, and source localisation among other numerous applications [12].

*Correspondence: mmesbah@ieee.org

¹University of Queensland Centre for Clinical Research, The University of Queensland, Brisbane, QLD 4029, Australia

²School of Mechanical and Chemical Engineering, The University of Western Australia, 35 Stirling Highway, Crawley, Perth, WA 6009, Australia
Full list of author information is available at the end of the article

Seizures appear in EEG as sudden, repetitive, evolving, stereotyped waveforms that last at least 10 s and have a definite beginning, middle, and end [13]. Their frequency-content varies with time [14–16] and is, therefore, best represented in the joint time–frequency domain instead of either the time domain or the frequency domain. Time–frequency methods, such as quadratic time–frequency distributions (TFDs) [17], facilitate the analysis of EEG seizure signals by exploiting their spectral energy variation with time.

Electroencephalogram patterns in neonatal seizures are highly variable with complex and varied morphology, frequency, and topography [18]. In this study, we analysed newborn EEGs using a quadratic TFD with separable kernel to characterise seizures in the time–frequency domain. We extracted the instantaneous frequency (IF) from the TFD to determine its modulation law; an important descriptive characteristic of EEG seizure [14–16,19,20]. The IFs were extracted using a method designed specifically for multi-component signals [21] and applied to a separable kernel TFD with optimised parameters. These extracted IFs were fitted to the four frequency modulated (FM) models previously linked with newborn EEG seizure [14,21]. To further characterise the extracted IFs, we computed their mean frequency and frequency span. Characterisation of newborn EEG seizures is an essential step in a number of applications such as modelling [16,22] and detection/classification [15,19,20].

Time–frequency signal processing

Time–frequency signal processing arose due to the need for accurate representation and efficient analysis and processing of nonstationary signals [17]. Nonstationary signals are very common natural phenomena. They are characterised by their time-varying frequency content which make them unsuitable for analysis by traditional methods, such as Fourier transform, that assume stationarity. Time–frequency signal analysis uses TFDs to represent signals in the joint time–frequency domain and is, therefore, capable of tracking signals' spectral change over time.

Quadratic time–frequency distributions

Quadratic TFDs have been extensively used in the analysis and processing of nonstationary signals in a number of practical applications. They can be mathematically formulated as [17]:

$$\rho_z(t, f) = W_z(t, f) \underset{(t, f)}{**} \gamma(t, f) \quad (1)$$

where $\rho_z(t, f)$ denotes the TFD, $W_z(t, f)$ the Wigner–Ville distribution (WVD), $\gamma(t, f)$ the time–frequency kernel, and $*$ the linear convolution operation. The above formulation can also be given in any of the other three joint domains [time-lag (t, τ) , Doppler-frequency (ν, f) , and

Doppler-lag (ν, τ)] that are linked to the time–frequency domain via the Fourier transform [17]. With a time–frequency kernel defined by $\gamma(t, f) = \delta(t)\delta(f)$, where δ is the Dirac delta function, the WVD is the most basic member of the quadratic class. For a real-valued signal $s(t)$, the WVD is defined as [17,23]:

$$W_z(t, f) = \int_{-\infty}^{\infty} z(t + \frac{\tau}{2}) \bar{z}(t - \frac{\tau}{2}) e^{-j2\pi f\tau} d\tau \quad (2)$$

where $z(t)$ is the analytic associate of $s(t)$ and \bar{z} is its complex conjugate. WVD possesses many desirable mathematical properties and provides the best joint time–frequency resolution among all quadratic TFDs for linear FM (frequency-modulated) signals [17]. However, being quadratic in nature, WVD introduces artefacts, or cross-terms, in the case of multi-component signals and nonlinear FM signals. The presence of these artefacts can mask the true signal components and make the interpretation of the TFD a difficult task.

Other members of the quadratic TFD class can be represented as filtered versions of the WVD, where their kernels act as two-dimensional smoothing filters [see (1)]. By carefully choosing the kernel, a quadratic TFD will be able to attenuate the cross-terms while maintaining some of the desirable properties of the WVD. As such, the proper selection of the TFD kernel and its parameters is an essential step in any TFD-based analysis and processing. There is a special class of kernels, referred to as separable kernels [24], whose members are expressed as the product of two single-variable functions; that is, as $\gamma(t, f) = g(t)H(f)$. This formulation makes the kernel design process easier and allows the smoothing in time and frequency directions to be independently performed.

Instantaneous frequency

Instantaneous frequency is an important feature characterising nonstationary signals. For a mono-component signal $s(t)$, with $z(t) = a(t)e^{j\varphi(t)}$ as its analytic associate, the IF is defined as [25]:

$$f(t) = \frac{1}{2\pi} \frac{d\varphi(t)}{dt} \quad (3)$$

where $a(t)$ is instantaneous amplitude and $\varphi(t)$ is the instantaneous phase. Many IF estimating techniques have been proposed in the literature and an extensive review can be found in [26]. As most TFDs exhibit a peak about the IF, one way to estimate the IF of mono-component signals is through the detection of these TFD peaks.

For a multi-component signal, consisting of a sum of two or more mono-component signals, the notion of a single IF becomes inappropriate. To characterise this type of signals, each mono-component is assigned its own IF. Among several IF estimation methods specifically

designed for multi-component signals that were previously proposed by some of the authors of this article in [21,27], the method in [21] is selected; it estimates IFs of multi-component signals by detecting and linking the local peaks of the TFD. This method has the advantage of not requiring prior knowledge about the signal under analysis except that its components are clearly separated in the time–frequency (TF) domain; a condition often satisfied by newborn EEG signals. The method has been successfully applied to biomedical signals such as EEG and ECG [20,28,29]. As seizure signals mostly have a high signal-to-noise (SNR) ratio [16,22], we decided to use this more established method for IF estimation rather than, for example, using the more recently proposed method for extracting IF from signals with low SNR [27]. More details on the IF estimation method is given in Section “Methods”.

Modelling of newborn EEG seizure in TF domain

Given an IF parametrised by $f(t, \Psi)$, where Ψ is an M -dimensional parameter vector, a class of single component nonstationary signals can be defined as [30]:

$$s(t) = a(t)e^{j2\pi \int_{-\infty}^t f(t, \Psi) d\tau} \quad (4)$$

In the present study, we used four classes of IF laws to characterize newborn EEG seizures. Besides the three classes previously identified [14,21], we added a new class, namely the hyperbolic FM class, as we observed some hyperbolic IF laws for newborn EEG seizures in our database. The IF models, $f(t, \Psi)$, along with the set of parameters, Ψ , for these classes are given in Table 1 [16,21,31]. For the LFM class, f_0 is the start (base) frequency and f_r is the frequency slope. For the SFM class, f_c is the carrier frequency, m is the amplitude of the cos component, and θ is the phase of the cos component. For the PWLFM class, $\alpha_2, \alpha_{1/2}, \alpha_{2/2}$ are slope values for the three pieces and B_1, B_2, f_m relate to the length of the pieces. For the HFM class, f_o is the starting (base) frequency and f_r is the slope of the pieces. More details can be found in [21,31].

Table 1 Frequency modulated (FM) classes: linear FM (LFM), sinusoidal FM (SFM), piecewise linear FM (PWLFM), and hyperbolic FM (HFM)

Name	IF law, $f(t)$	Parameter set, Ψ
LFM	$f_0 + f_r t$	$[f_0, f_r]$
SFM	$f_c + m \cos(2\pi f_m t + \theta)$	$[f_c, m, f_m, \theta]$
PWLFM	$(\alpha_1 - \alpha) t - B_1 + (\alpha - \alpha_2) t - B_2 $ $+ \alpha_1(t - B_1) + \alpha_2(t - B_2) + f_m$	$[\alpha, \alpha_1, \alpha_2, B_1, B_2, f_m]$
HFM	$f_0/(1 + f_r t)$	$[f_0, f_r]$

Methods

We classified the newborn EEG seizure components based on their parametric IF models using the following process. First, IFs of seizure components were obtained using an IF estimation method specifically designed for nonstationary multi-component signals [21]. This method starts by mapping the time-domain EEG signals into the time–frequency domain using a suitably chosen quadratic TFD and followed by TFD local peak detection and component linking operations. Each extracted IF is then fitted to the above four parametric models using a large scale nonlinear least squares algorithm [32,33]. The seizure pattern is finally assigned to the class represented by the parametric IF model that best fits, in the least mean squared error sense, the IF extracted from the seizure component. The following gives more details about this three-stage process.

Step 1: TF transformation

A suitable choice of a TFD depends on the application. To account for the nonstationary and multi-component nature of newborn EEG, the selected TFD should provide high spectral resolution and have good cross-term reduction capability. In this study, we chose a separable kernel TFD defined by the following time–frequency kernel:

$$\gamma(t, f) = g(t)H(f)$$

where $g(t)$ is the smoothing window, whose window length controls the trade-off between time resolution and cross-term reduction. And $H(f)$ is the Fourier transform of the analysis window $h(\tau)$ whose length controls the trade-off between frequency resolution and inner-artefacts reduction [30].

We used the separable kernel in this study to: (1) suppress cross-terms and localise the signal components in the time–frequency domain [21,24] and (2) obtain an accurate IF estimation [21]. This kernel-type was previously shown to be particularly suitable for newborn EEG signals [19,34]. In this study, we tested three separable kernel TFDs to select the best one for representing the newborn EEG. The discrete-time versions of these kernels in the Doppler-Lag domain are given in Table 2, where $g(n)$ is the discrete Fourier transform of $g(t)$ and $h(m)$ is the discrete-time version of $h(\tau)$. Also, Γ is the gamma function, β is a smoothing parameter, and σ is a measure of the spread of the Gaussian window. The lengths of the Hann and Hamming windows are $N + 1$ and $M + 1$, respectively.

Step 2: TFD local peaks detection and component linking

The TFD can be regarded as a two-dimensional image with time and frequency as its row and column coordinates. Local maxima (with respect to frequency) are identified using both the first and second derivative tests.

Table 2 Separable kernels used in the TFD selection process

Kernel	$g(n)$	$h(m)$	Parameters (a, b)
Hann–Hamming	$0.54 + 0.5 \cos\left(\frac{2\pi n}{N}\right)$	$0.54 + 0.46 \cos\left(\frac{2\pi m}{M}\right)$	(N, M)
Hann–Gaussian	$0.54 + 0.5 \cos\left(\frac{2\pi n}{N}\right)$	$\exp\left(-\frac{m^2}{2\sigma^2}\right)$	(N, σ)
Modified-B–Hamming	$\frac{ \Gamma(\beta + jn) ^2}{\Gamma(\beta)}$	$0.54 + 0.46 \cos\left(\frac{2\pi m}{M}\right)$	(β, M)

Only those local maxima that satisfy the condition of $\eta \max \rho_z(t, f)$ where η is a prefixed threshold, are considered as valid peaks. By assigning value 1 to the locations of valid peaks and value 0 to all others, the TF image is transformed into a binary image $B(t, f)$ [21]:

$$B(t, f) = \begin{cases} 1, & \text{if } \left\{ \frac{\partial \rho_z(t, f)}{\partial f} = 0 \right\} \text{ and } \left\{ \frac{\partial^2 \rho_z(t, f)}{\partial f^2} < 0 \right\} \\ & \text{and } \left\{ \rho_z(t, f) > \eta \max \rho_z(t, f) \right\} \\ 0, & \text{otherwise.} \end{cases}$$

Ideally, the IF of a signal component along which the signal energy concentrates is presented in the TFD as a ridge. The component linking algorithm detects a linked component in $B(t, f)$ by examining the pixel connectivity and the number of connected pixels. Among the sets of connected pixels, only those with number of pixels exceeding a preset threshold are identified as true linked components of seizure IFs. To eliminate IFs of non-seizure components, this threshold is set to the minimum time duration of a seizure component in samples. For this study, we set this minimum threshold to 10 s [13].

Step 3: fitting and classifying the IF models

Each IF parametric model was fitted to the extracted IF. The parameters for each model were optimised to give the lowest mean squared error. We used the trust-region-reflective algorithm to solve the nonlinear least-squares problem [32,33]. This algorithm is a subspace iterative trust region method for solving large scale nonlinear least squares problems. Trust region methods are robust optimisation methods with strong convergence properties. To guarantee that the iterates stay within the strictly feasible (trust) region, an interior-reflective technique is used. The resulting method, which can be considered as a natural generalization of the trust region method for unconstrained optimization, overcomes the problem and has relatively good computational performance. The IF model with the lowest mean squared error was considered the best fit for the estimated IF.

Data acquisition

The EEG data used in our study were collected from 35 newborns, admitted to the Royal Brisbane and Women's Hospital, Brisbane, Australia, using the MEDELEC Profile system (Medelec, Oxford Instruments, UK). The 20-channel EEG recordings were obtained using the standard 10–20 International System of Electrode Placement [35]

with a bipolar montage (see Table 3). The EEG was filtered with a [0.5–70] Hz band-pass filter prior to sampling at a rate of 256 Hz. The periods of newborn EEG with seizure activities were identified by a neurologist from the Royal Children's Hospital, Brisbane, Australia. All the recordings were acquired in the presence of a trained technician who recorded the different behaviours that may affect the interpretation of the EEG such as degree of comfort (comfortable, irritable), apparent mental status (sleep, awake, alert, nonresponsive), feeding (type and route), physical behaviour (body position) and medical treatments (limb restraints, intubation). Previous studies [36] showed that over 95% of the spectral energy of newborn EEG resides in Delta (0.5–4 Hz) and Theta (4–8 Hz) frequency bands. Therefore, the EEG data was further filtered with a 13 Hz low pass filter and then down-sampled to 32 Hz to reduce computational cost. In this study, we used a total of 649 artefact-free EEG seizure epochs of 30-s duration each. We chose to use 30 s as a compromise between a good discriminating power of the IF feature and the computational cost. Longer epochs tend to give more complex IF morphology and, therefore, may require more complex FM laws and computational power. These epochs were extracted from multiple EEG channels, the specifics of which are given in Table 3. As harmonic components in newborn EEG seizure may be present [14], only the most energetic (fundamental) was considered in our analysis. We did not include the harmonic components as we found

Table 3 Distribution of the 649 seizure epochs from the 20-channel dataset

Left hemisphere		Right hemisphere	
Channel	Number of epochs	Channel	Number of epochs
4 (F3–T3)	20	1 (F4–T4)	28
5 (T3–T5)	37	2 (T4–T6)	23
6 (T5–O1)	24	3 (T6–O2)	27
10 (F3–C3)	26	7 (F4–C4)	21
11 (C3–P3)	29	8 (C4–P4)	34
12 (P3–O1)	35	9 (P4–O2)	42
15 (Cz–C3)	39	13 (T4–C4)	36
16 (C3–T3)	28	14 (C4–Cz)	50
19 (Pz–P3)	44	17 (T6–P4)	22
20 (P3–P5)	39	18 (P4–Pz)	45
Total	321	Total	328

that, in more than 75% of the cases, the energy of the fundamental component was more than twice as large as the first most energetic harmonic. Also, the energy ratio of the fundamental component to the second most energetic harmonic was larger than 3 in more than 87% of the cases.

Results and discussion

Figure 1 shows three different representations of a 30-s epoch of newborn EEG seizure obtained with the TFSA package [17], a toolbox for MATLAB. Compared to the time domain (left plot) and the frequency domain (bottom plot), the TFD (centre plot) provides a more informative description of the EEG seizure by revealing the temporal variation of its frequency content. Visual examination of the TFD suggests that there are one fundamental component and a number of harmonics, which supports previous findings about newborn EEG seizure [14,16]. Results of IF estimation are presented in Figure 2. The best IF model/class that characterizes the fundamental component is determined to be SFM as shown in Figure 2.

Selecting the optimal separable TFD

To select the best separable TFD to represent the EEG in the time–frequency plane, we had to select the optimal kernel parameters that give the most accurate IF estimate. As there is no way to access the true IFs of the real newborn EEG, the second best option was to run the optimization test on a simulated newborn EEG signals with known IFs. The most adequate and realistic EEG model for this task was the one previously proposed by some of the current authors [16]. The model consists of

background and seizure sub-models. The background model is based on the short-time power spectrum with a time-varying power law. The seizure model was designed to address most of the significant time–frequency characteristics of newborn EEG seizure such as multiple components (fundamental and harmonics), nonlinear IF FM law, and amplitude modulation. More details can be found in [16]. Most of the parameters of EEG models were shown to behave like random variables with beta or log-normal distributions. The EEG epoch is obtained by linearly combining the simulated seizure and background; that is

$$\text{eeg}(n) = \text{back}(n) + \text{SBR} \times \text{seiz}(n)$$

where $\text{back}(n)$ stands for EEG background, $\text{seiz}(n)$ for EEG seizure and SBR for seizure to background ratio; a parameter that plays a similar role to the SNR in the case of noisy signals. To select the optimal parameters of the three separable kernels, we performed a Monte Carlo simulation using the above model to generate 30-s realistic newborn EEG epochs with known IFs. As the parameters of the seizure IF model are mostly random variables and, therefore, change from iteration to another, we were not able to use the conventional criteria for the accuracy of an estimator, namely the bias and variance. We have used instead the following mean square error as a criterion to judge the performance of the TFD-based IF estimators

$$\text{mse}(a, b) = \frac{1}{P} \sum_{k=1}^P \frac{1}{L_k} \sum_{n=1}^{L_k} \left| \hat{f}_k(n; a, b) - f_k(n) \right|^2$$

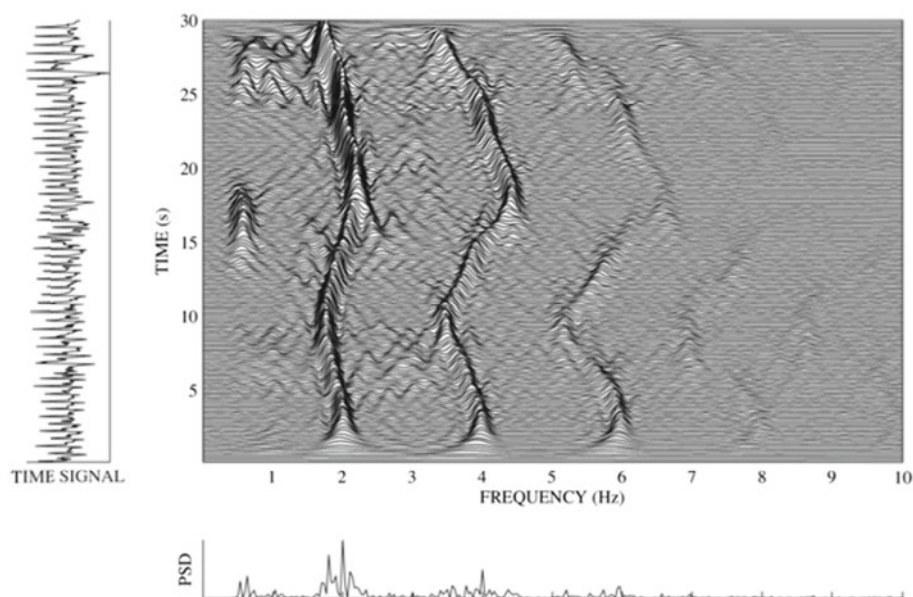


Figure 1 Example of newborn EEG seizure. Time plot, frequency plot (power spectral density, PSD), and TFD of 30-s newborn EEG.

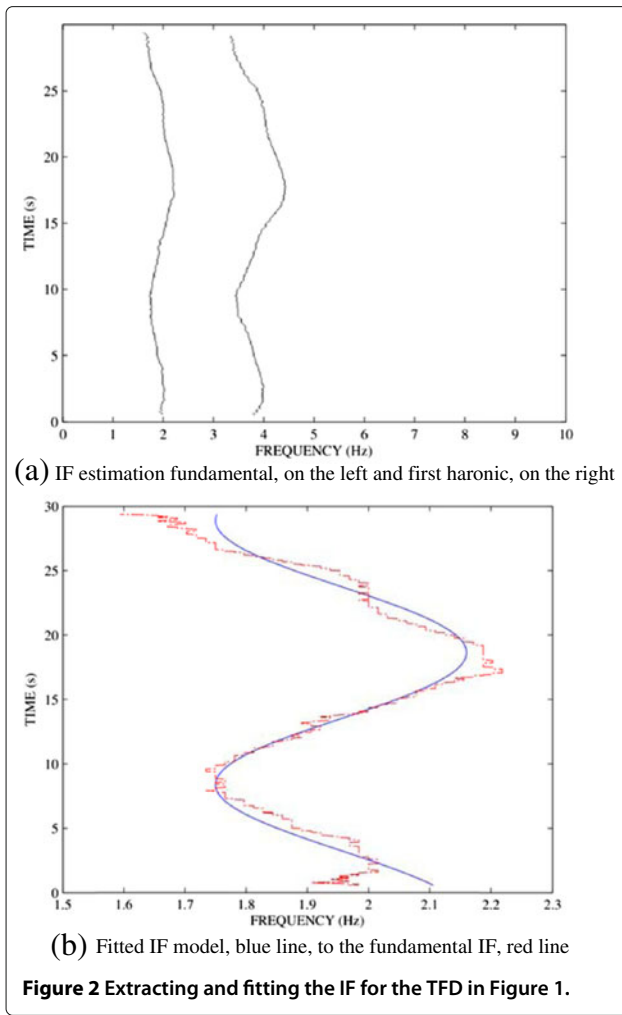


Figure 2 Extracting and fitting the IF for the TFD in Figure 1.

where (a, b) are the parameters of the kernel (see Table 2), P is the total number of Monte Carlo iterations, $\hat{f}_k(n; a, b)$ is the estimated IF of length L_k computed using the multicomponent IF estimator at the k -th iteration for given parameters (a, b) and $f_k(n)$ is the true IF of the simulated seizure at the k -th iteration. The optimal kernel parameters were selected such that

$$(a_{\text{opt}}, b_{\text{opt}}) = \arg \min_{(a, b)} \{ \text{mse}(a, b) \}$$

In this study, the following parameters have been used:

EEG model: Sampling frequency = 32 Hz, EEG epoch length = 30 s, and SBR = 10 dB.

IF estimation: Peak threshold $\eta = 0.01$ and minimum length of IF = 10 s. We studied different values of η larger than 0.01 but most of them failed to extract valid IFs.

Monte Carlo simulation: 50 iterations.

Separable kernels: 40 discrete kernel parameters values for both a and b .

The results of the Monte Carlo simulation are shown in Figure 3 and the minimum mean-MSE values are in Table 4.

Although the Hann–Gaussian kernel gives the best overall performance, the results of the three kernels are very close. We have also noticed that the IF estimators are not very sensitive to changes in the kernel parameters in the neighbourhood of the optimal values as can be seen in Figure 3. Based on these results, we chose the Hann–Gaussian separable kernel with parameters (77, 0.058) to perform the IF estimation for the newborn EEG seizure characterisation.

Fitting FM signal models

The bar chart in Figure 4a displays the results of IF classification. Out of the 649 seizure epochs, 392 (60.4%) epochs have IFs that are best modelled by a piece-wise linear FM, 211 (32.51%) by a sinusoidal FM law, 43 (6.63%) by hyperbolic FM and only 3 (0.46%) by a linear FM law. Because the 649 seizure signal components were collected from multiple channels of both left and right hemispheres, we examined the distribution of the IF classes related to each EEG channel and for the two hemispheres to check if there is any preferential tendencies. As shown in Figure 4b, the IF class distributions are quite similar in the two hemispheres.

The results of IF class distributions related to each EEG channel are shown in Figure 4c. Visual examination suggests that there are notable differences among channels. Piecewise-linear FM is still the class with the highest percentage in all channels followed by the sinusoidal FM. But in channel 12 (P3–O1) and channel 20 (P3–P5), the percentages of these two classes are close. In this channel, piecewise-linear FM class account for over 50% while sinusoidal FM class occupies about 45%. The percentage of piecewise-linear FM class and sinusoidal FM class in channel 20 (P3–P5) are approximately 44 and 41%, respectively. In other channels, the percentages of piecewise-linear FM class ranges from 55 to 68% while that of sinusoidal FM class is between 25 and 40%. Channel 7 (F4–C4) has the highest percentage (around 19%) of hyperbolic FM signal components among all the channels. Channels 2 (T4–T6), 8 (C4–P4), 16 (C3–T3), 17 (T6–P4) and 20 (P3–P5) also have a relatively high percentage (over 10%) of hyperbolic FM components compared to the rest of the channels. The linear FM signal components were only found in Channels 1 (F4–T4), 3 (T6–O2), 9 (P4–O2) and 10 (F3–C3) at low percentages. For objective comparisons, we used a pair-wise Fisher's exact test between the two hemispheres. At a significance level of 0.05, left and right hemispheres were not found to be significantly different.

Another finding worth mentioning is that when checking the intermediate results of IF class distributions, we

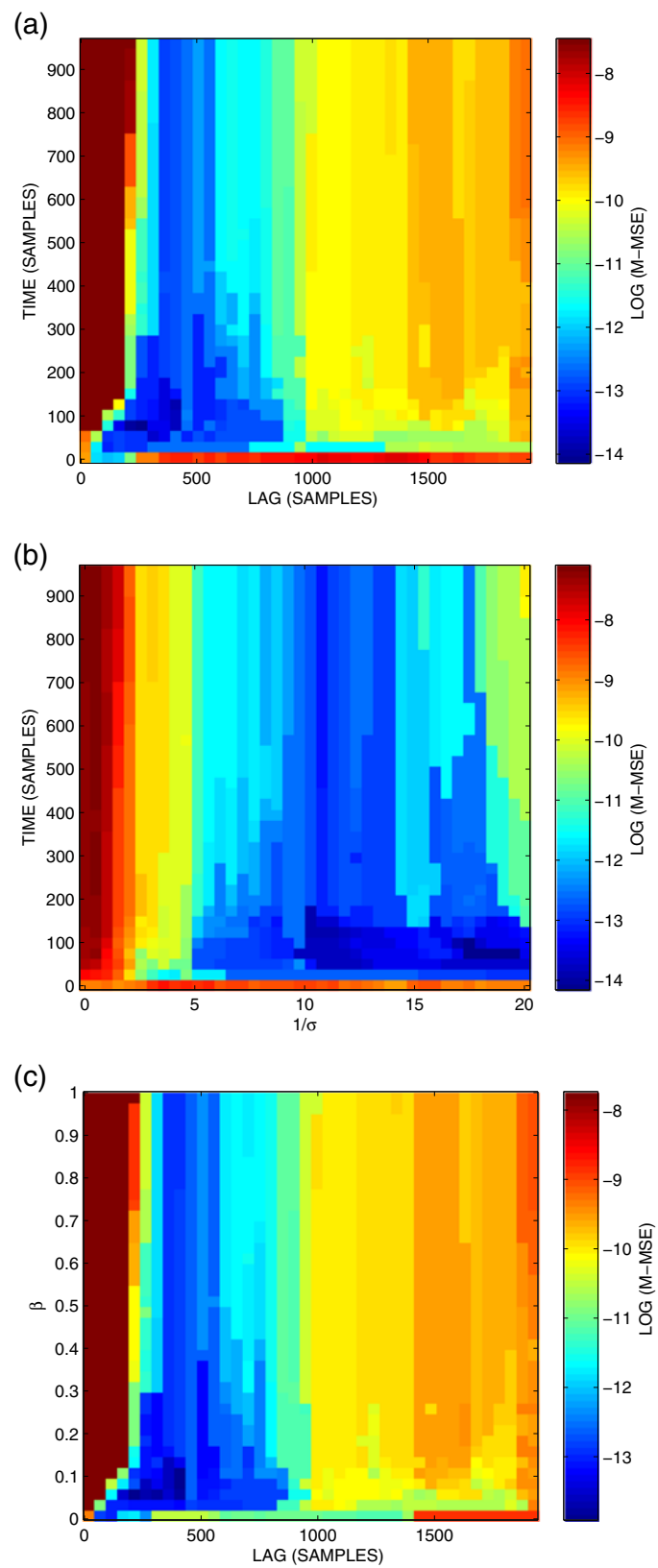


Figure 3 Results of Monte Carlo simulations. Plots uses the log value of the mean mean-squared-error (M-MSE) to highlight the small changes over the parameter values.

Table 4 Distribution of the 649 seizure epochs from the 20-channel dataset

Kernel	Optimal parameters (a_{opt} , b_{opt})	Minimum mean-MSE
Hann-Hamming	(77,265)	7.205×10^{-7}
Hann-Gaussian	(77,0.058)	7.093×10^{-7}
Modified-B-Hamming	(0.06,215)	9.061×10^{-7}

found that in all the cases where the EEG seizure component was assigned to the linear FM class, the mismatch errors (MSE) resulting from selecting the linear FM model and the piecewise linear FM model were very close. This is expected as the piecewise linear FM model is flexible enough to account for the simple LFM case. Also, the infrequent occurrence of linear FMs is because of the complexity of the EEG seizure behaviour over relatively long windows; a factor that was found to limit the performance of automatic seizure detection when using EEG epochs larger than 12 s. Also, but to a lesser degree, we found that when the hyperbolic FM model was selected as the best fit, the difference between MSE associated with hyperbolic FM and sinusoidal FM were small. These observations suggest that EEG seizure epochs can be practically characterized by two classes, namely piecewise linear FM and sinusoidal FM.

Quantifying the IF

The characteristics of newborn EEG seizure components were further studied by analysing their mean frequencies and frequency spans over the 30 s epochs. The mean frequency was calculated as the average frequency of the estimated fundamental IF and frequency span as the difference between the maximum frequency and minimum frequency of this estimated IF. Box-and-whisker plots were used to provide a visual summary of their distributions. The results are shown in Figures 5 and 6.

Figures 5a and 6a present the distributions of mean frequencies and frequency ranges extracted from all the 649 signal components. The mean frequencies of the EEG seizure components range from about 0.6 to 6.5 Hz (mean: 1.58, standard deviation: 0.72), with most of epochs' mean frequency in the Delta frequency band (0.5–4 Hz). They are, however, not evenly spread across the entire range, with the first 25% between 0.6 and 1.1 Hz, the second 25% grouping more closely in the range 1.1–1.4 Hz, the third 25% between 1.4 and 1.9 Hz and the rest spreading more sparsely towards the higher frequencies.

Most of the EEG seizure epochs' IF components have frequency span in the range of 0.15–1 Hz, and a few have larger frequency spans beyond 1 Hz. Similar to the mean frequency, the distribution of frequency span is slightly skewed towards the right, with the lower adjacent value at around 0.15 Hz, the first quartile at about 0.38 Hz,

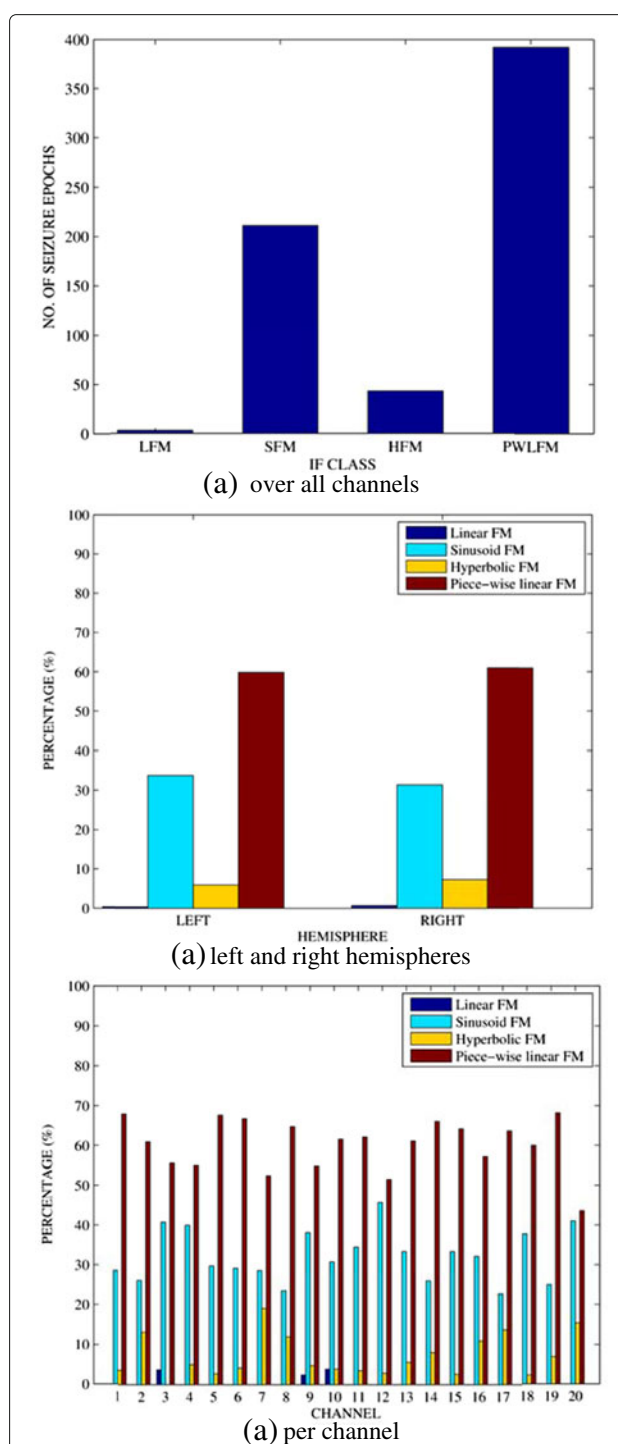


Figure 4 Classification results for the FM signals. (a) Over all channels. (b) Left and right hemisphere.

the median at 0.5 Hz, the third quartile at approximately 0.65 Hz and the upper adjacent value at about 1 Hz. These mean frequency and frequency span results agree with previous findings, such as studies in [14,16], which

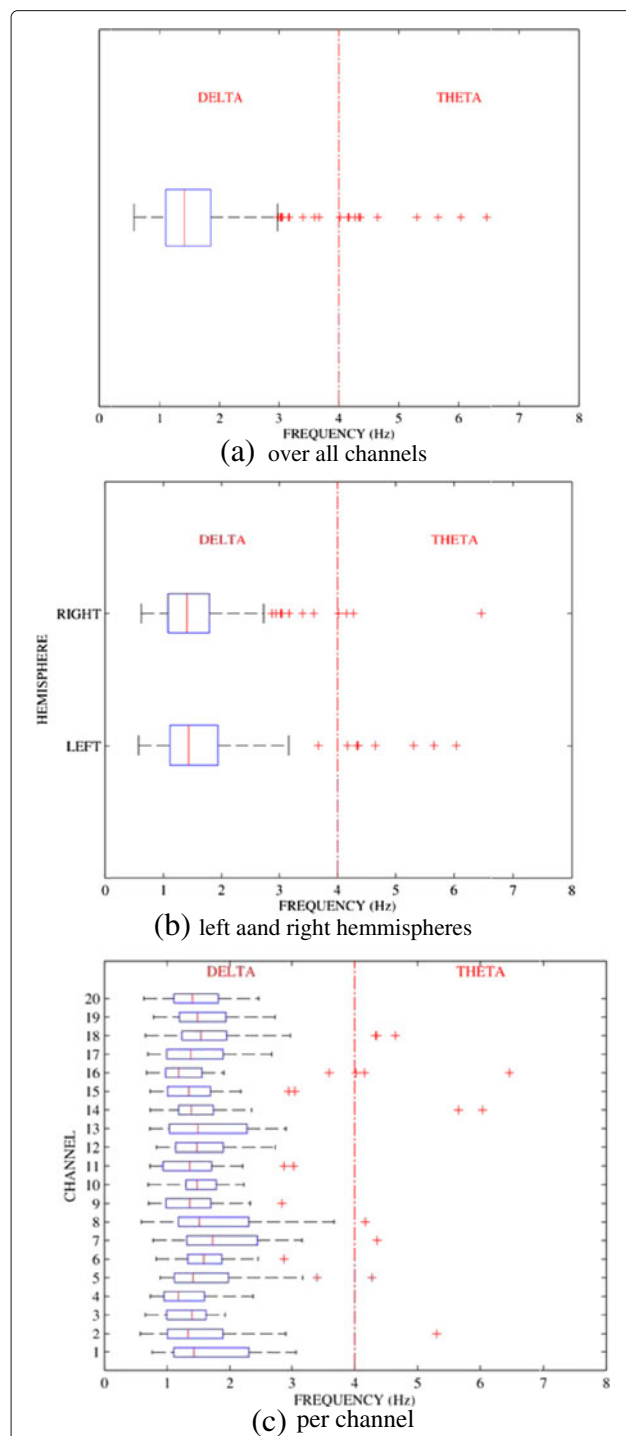


Figure 5 Mean-frequency of fundamental IF. For each box, the central line represents the median, the edges of the boxes represent the 25th and 75th percentile, the whiskers represent the extreme points, and the outliers are plotted as separate data points.

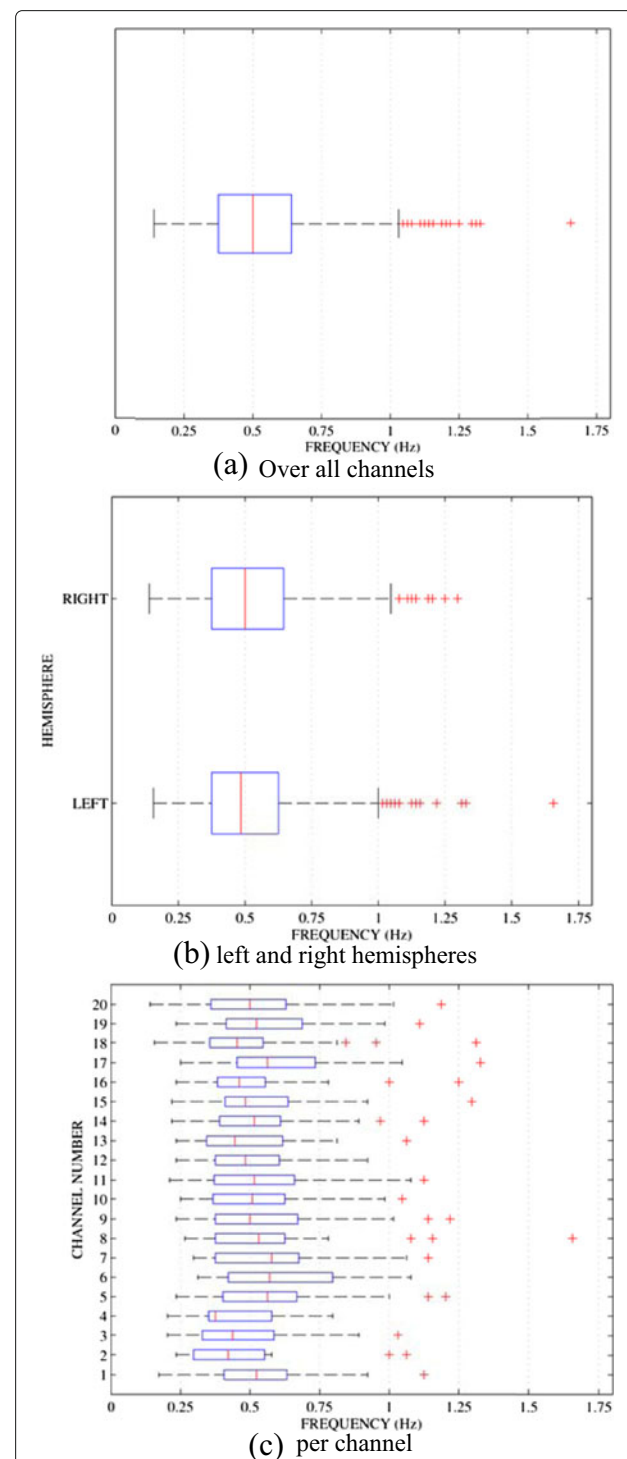


Figure 6 Frequency span (maximum to minimum values) of fundamental IF for 30-s epochs. For each box, the central line represents the median, the edges of the boxes represent the 25th and 75th percentile, the whiskers represent the extreme points, and the outliers are plotted as separate data points.

constrains seizure energy to the first 5 Hz frequency band. The difference in the higher frequency end (that is, 3–5 Hz) can be explained by the fact that we have ignored the relatively low energy harmonics that reside in frequencies higher than 3 Hz.

To find out if there are differences among different brain regions in terms of mean frequency and frequency span distributions, we performed the same analysis as before but this time grouping the channels in hemispheres. In Figures 5b and 6b the distributions of the mean frequencies and the frequency spans were plotted for comparisons between hemispheres and among channels. These results suggest that the left and right hemispheres are quite similar in terms of both mean frequency distributions and frequency span distributions. The distributions of both mean frequencies and frequency spans from both hemispheres are slightly skewed towards the high frequency, though slightly more in the right hemisphere and in the case of mean frequency distributions. An objective comparison between hemispheres using Mann–Whitney *U*-tests [37] showed that there was no significant difference for mean frequency ($p = 0.1860$) and the frequency span ($p = 0.3022$), applying a significance level of 0.05.

The mean frequency and frequency span distributions of seizure signal components in each channel are presented in Figures 5c and 6c. Similar to the combined distributions in Figures 5a and 6a, all the channels have a mean frequency mostly within the Delta frequency band, and frequency spans within a 0.15–1 Hz range.

It is not accurate to do the comparisons among channels just by means of visual inspection. But some channels do stand out from the rest. Each of the channels 2 (T4–T6), 5 (T3–T5), 7 (F4–C4), 8 (C4–P4), 14 (C4–Cz), 16 (C3–T3) and 17 (T6–P4) has no more than three seizure components of higher mean frequencies within the theta frequency band, which are marked as outliers. Ignoring outliers in the distributions, the mean frequencies of signal components in Channels 3 (T6–O2) and 16 (C3–T3) are tightly grouped in much smaller frequency bands compared to others, while the mean frequencies in Channel 8 (C4–P4) spread across the widest range among all the channels. Compared to other channels, the frequency ranges of seizure signal components in Channel 2 (T4–T6) are restricted in a much small range when disregarding the two outliers.

Quantifying the mean- and frequency-span parameters is important for improving existing, and developing new, seizure detection methods. For example, a time-frequency matched filter approach builds a template set from a model of seizure IF; knowing the type of IF signal model, and the distribution of seizure IF frequencies, will help to build more accurate template sets for this method [15,19].

Conclusions

In this study, we characterised newborn EEG seizures using the fundamental IFs extracted from the UQCCR database of 35 newborns. Among the identified four IF law classes of newborn EEG seizures, the piecewise FM and the sinusoidal FM classes appeared to be the most frequent. Depending on the brain region, the two classes accounted for about 80 to 98% of all the seizure components. For the frequency of occurrence of the different classes, no significant difference was found between different brain regions. The mean frequencies and frequency spans of about 95% of seizure components from the newborn EEG seizure dataset were found to be in the range of 0.6–3 Hz and 0.2–1 Hz, respectively. Similar to the case of class distributions, no significant differences were found between the two hemispheres in terms of mean frequencies and frequency spans of the EEG seizure components.

In the attempt to characterize newborn EEG seizures, we focused the study on modelling the fundamental IF and extracting mean frequency and frequency span values for the estimated fundamental IFs, all within a 30-s epoch. This information will be useful when constructing new nonstationary methods for automatic detection and classification of seizure or for improving existing methods such as [19,20]. This study was not exhaustive as there are other aspects of the seizure components that can be investigated as potential discriminating features. Some of these are the amplitude modulation, ratio of energy of the fundamental to the harmonic components, the time duration, the number of harmonic components, and coherence of IF laws across channels. Also, the effect of different epoch lengths on the seizure characterization will need to be studied. The investigation of these features will be the subject of future work that aims at gaining more understanding about the different characteristics of newborn EEG seizures.

Competing interests

The authors declare that they have no competing interests.

Acknowledgements

The authors gratefully acknowledge the earlier contributions of Dr. Luke Rankine in algorithm development and Ms. Fangei Xu for generating the classification and statistical tests used in this article. The authors also acknowledge funding from the Qatar National Research Fund, Grant number NPRP 09-465-2-174 (after December 2010), and the Australian Research Council, Grant Number DP0665697 (prior to December 2010). In addition, one of the authors, Dr Mostefa Mesbah, wishes to acknowledge receiving a small preparation funding grant from UQ Firstlink Fund 2010.

Author details

¹University of Queensland Centre for Clinical Research, The University of Queensland, Brisbane, QLD 4029, Australia. ²School of Mechanical and Chemical Engineering, The University of Western Australia, 35 Stirling Highway, Crawley, Perth, WA 6009, Australia. ³DeustoTech, University of Deusto, Bilbao 48013, Spain. ⁴College of Engineering, Qatar University, Doha, Qatar.

Received: 15 December 2011 Accepted: 5 June 2012

Published: 13 July 2012

References

1. C Lombroso, Neonatal seizures: historic note and present controversies. *Epilepsia*. **37**(s3), 5–13 (1996)
2. J Volpe, Neonatal Seizures. in *Neurology of the Newborn*. 4th edn., ed. by Volpe J. (Philadelphia: W.B. Saunders, 2000)
3. C Hahn, J Riviello Jr., Neonatal seizures and EEG: electroclinical dissociation and uncoupling. *NeuroReviews*. **5**(8), e350 (2004)
4. R Fisher, W Boas, W Blume, Epileptic seizures and epilepsy: definitions proposed by the International League Against Epilepsy (ILAE) and the International Bureau for Epilepsy (IBE). *Epilepsia*. **46**(4), 470–472 (2005)
5. G Holmes, Childhood-Specific Epilepsies Accompanied by Developmental Disabilities: Causes and Effects. in *Epilepsy and developmental disabilities*, ed. by Devinsky O and Westbrook L. (Chatsworth, Australia: Elsevier, 23–32, 2001)
6. A Hill, Neonatal seizures. *Pediatr. Rev.* **21**(4), 117–121 (2000)
7. W Deburghgraeve, PJ Cherian, M De Vos, RM Swarte, JH Blok, GH Visser, P Govaert, S Van Huffel, Automated neonatal seizure detection mimicking a human observer reading EEG. *Clin. Neurophysiol.* **119**(11), 2447–2454 (2008)
8. A Malone, C Anthony Ryan, A Fitzgerald, L Burgoyne, S Connolly, G Boylan, Interobserver agreement in neonatal seizure identification. *Epilepsia*. **50**(9), 2097–2101 (2009)
9. D Murray, G Boylan, I Ali, C Ryan, B Murphy, S Connolly, Defining the gap between electrographic seizure burden, clinical expression and staff recognition of neonatal seizures. *Arch. Dis. Child. Fetal Neonatal Ed.* **93**(3), F187 (2008)
10. MS Scher, Electroencephalography of the Newborn: Normal and Abnormal Features. in *Electroencephalography: Basic Principles, Clinical Applications, and Related Fields*. 5th edn., ed. by Niedermeyer E and Silva FLD. (Philadelphia, USA: Lippincott Williams & Wilkins, 937–989, 2004)
11. M Thibeault-Eybalin, A Lortie, L Carmant, Neonatal seizures: do they damage the brain? *Pediatr. Neurol.* **40**(3), 175–180 (2009)
12. S Sanei, J Chambers, *EEG Signal Processing*. (Chichester, UK: John Wiley & Sons, 2007)
13. JS Hahn, BR Tharp, Neonatal and Pediatric Electroencephalography. in *Electrodiagnosis in Clinical Neurology*, ed. by Aminoff MJ. (New York: Elsevier Churchill Livingstone, 85–129, 2005)
14. B Boashash, M Mesbah, A time–frequency approach for newborn seizure detection. *IEEE Eng. Med. Biol. Mag.* **20**(5), 54–64 (2001)
15. B Boashash, M Mesbah, Time–Frequency Methodology for Newborn Electroencephalographic Seizure Detection. in *Applications in Time–Frequency Signal Processing*, ed. by Papandreou-Suppappola A. (Boca Raton, Florida: CRC Press, 339–369, 2002)
16. L Rankine, N Stevenson, M Mesbah, B Boashash, A nonstationary model of newborn EEG. *IEEE Trans. Biomed. Eng.* **54**, 19–28 (2007)
17. B Boashash, (ed.), *Time–Frequency Signal Analysis and Processing: A Comprehensive Reference*. (Oxford, UK: Elsevier, 2003)
18. D Shewmon, What is a neonatal seizure? Problems in definition and quantification for investigative and clinical purposes. *J. Clin. Neurophysiol.* **7**(3), 315 (1990)
19. JM O’ Toole, B Boashash, Time–frequency detection of slowly varying periodic signals with harmonics: methods and performance evaluation. *EURASIP J. Adv. Signal Process.* **2011**(Article ID 193797), 1–16 (2011)
20. NJ Stevenson, JM O’Toole, LJ Rankine, GB Boylan, B Boashash, A nonparametric feature for neonatal EEG seizure detection based on a representation of pseudo-periodicity. *Med. Eng. Phys.* **34**(4), 437–446 (2012)
21. L Rankine, M Mesbah, B Boashash, IF estimation for multicomponent signals using image processing techniques in the time–frequency domain. *Signal Process.* **87**(6), 1234–1250 (2007)
22. NJ Stevenson, M Mesbah, GB Boylan, PB Colditz, B Boashash, A nonlinear model of newborn EEG with nonstationary inputs. *Ann. Biomed. Eng.* **38**(9), 3010–3021 (2010)
23. B Boashash, Note on the use of the Wigner distribution for time–frequency signal analysis. *IEEE Trans. Acoust. Speech Signal Process.* **36**(9), 1518–1521 (1988)
24. B Boashash, GR Putland, Design of, High-Resolution Quadratic TFDs with Separable Kernels. in *Time–Frequency Signal Analysis and Processing: A Comprehensive Reference*, ed. by Boashash B. (Oxford, UK: Elsevier, 213–222, 2003)
25. B Boashash, Estimating and interpreting the instantaneous frequency of a signal—part 1: fundamentals. *Proc. IEEE*. **80**(4), 520–538 (1992)
26. B Boashash, Estimating and interpreting the instantaneous frequency of a signal—part 2: algorithms and applications. *Proc. IEEE*. **80**(4), 540–568 (1992)
27. J Lerga, V Susic, B Boashash, An efficient algorithm for instantaneous frequency estimation of nonstationary multicomponent signals in low SNR. *EURASIP J. Adv. Signal Process.* **2011**(Article ID: 725189), 1–16 (2011)
28. MB Malarvili, M Mesbah, Newborn seizure detection based on heart rate variability. *IEEE Trans. Biomed. Eng.* **56**(11), 2594–603 (2009)
29. S Dong, M Mesbah, BE Lingwood, JM O’ Toole, B Boashash, Time–frequency analysis of heart rate variability in neonatal piglets exposed to hypoxia. in *Proc. of Computing in Cardiology Conf.* (Hangzhou, China, 701–704, 2011)
30. B Boashash, Time–Frequency, Signal Analysis. in *Advances in Spectrum Estimation*, ed. by Haykin S. (Englewood Cliffs, NJ: Prentice-Hall, 418–517, 1991)
31. P Celka, P Colditz, Nonlinear nonstationary Wiener model of infant EEG seizures. *IEEE Trans. Biomed. Eng.* **49**(6), 556–564 (2002)
32. T Coleman, Y Li, On the convergence of interior-reflective Newton methods for nonlinear minimization subject to bounds. *Math. Progr.* **67**, 189–224 (1994)
33. T Coleman, Y Li, An interior trust region approach for nonlinear minimization subject to bounds. *SIAM J. Opt.* **6**, 418–445 (1993)
34. JM O’ Toole, Discrete quadratic time–frequency distributions, definition, computation, and a newborn electroencephalogram application. PhD thesis, School of Medicine, The University of Queensland, 2009, <http://espace.library.uq.edu.au/view/UQ:185537>
35. H Jasper, The ten–twenty electrode system of the international federation. *Electroencephalogr. Clin. Neurophysiol.* **10**(2), 371–375 (1958)
36. M Scher, M Sun, D Steppe, R Guthrie, R Scabassi, Comparisons of EEG spectral and correlation measures between healthy term and preterm infants. *Pediatr. Neurol.* **10**(2), 104–108 (1994)
37. D Stengel, M Bhandari, M Hanson, *Statistics and Data Management: A Practical Guide for Orthopedic Surgeons*. (New York: Thieme Medical Pub, 2010)

doi:10.1186/1687-6180-2012-143

Cite this article as: Mesbah et al.: Instantaneous frequency based newborn EEG seizure characterisation. *EURASIP Journal on Advances in Signal Processing* 2012 **2012**:143.

Submit your manuscript to a SpringerOpen[®] journal and benefit from:

- Convenient online submission
- Rigorous peer review
- Immediate publication on acceptance
- Open access: articles freely available online
- High visibility within the field
- Retaining the copyright to your article

Submit your next manuscript at ► springeropen.com